Phase diagram of the quadrumerized Shastry-Sutherland model

Andreas Läuchli, Stefan Wessel, and Manfred Sigrist
Institut für Theoretische Physik, ETH-Hönggerberg, CH-8093 Zürich, Switzerland
(Received 5 February 2002; published 20 June 2002)

We determine the phase diagram of a generalized Shastry-Sutherland model, using a combination of dimer- and quadrumer-boson methods and numerical exact diagonalization techniques. Along special lines in the parameter space the model reduces to the standard Shastry-Sutherland model, the 1/5th depleted square lattice and the two-dimensional plaquette square lattice model. We study the evolution of the ordered phases found in the latter two unfrustrated models under the effect of frustration. Furthermore we present exact diagonalization results for the Shastry-Sutherland model on clusters with up to 32 sites, supporting the existence of an intermediate gapped valence bond crystal phase with plaquette long-range order.

DOI: 10.1103/PhysRevB.66.014401 PACS number(s): 75.10.Jm, 75.40.Mg

There has been considerable interest in recent years in the study of low-dimensional quantum spin systems, both experimentally and theoretically. Special attention has been devoted to two-dimensional antiferromagnetic systems, where quantum fluctuations and frustration allow for various exotic quantum phases to compete with quasiclassical long-range magnetic order.[1]

Already in the unfrustrated regime such spin liquid phases occur in certain regions of the parameter space, a prominent example being the spin-1/2 Heisenberg model on the 1/5th depleted square lattice.[2] In this model two distinct spin liquid phases, well described by resonating valence bond (RVB) -like states, are found along with an intermediate long-range antiferromagnetically ordered phase.[2,3] The location of the quantum critical points separating these phases is known to rather high precision.[4]

When considering frustrated systems, ground-state properties are less well established. A prominent example of recent interest, due to its relevance for the spin gap system $SrCu_2(BO_3)_2$,[5,6] is the Shastry-Sutherland model (SSM).[7] In this model the nearest-neighbor square lattice antiferromagnet is frustrated by additional diagonal interactions, arranged in a staggered pattern on alternate squares. This model retains long-range Néel order for small diagonal coupling. Furthermore, it becomes an exact dimer valence bond solid (VBS) with singlets forming on the diagonal bonds for small axial coupling. Concerning the existence and nature of intermediate phases, despite numerous investigations,[8–12] a definite picture has not yet emerged.

I. THE MODEL

In this paper, we present exact diagonalization studies on the SSM that indicate the occurrence of a valence bond crystal (VBC) in the intermediate regime, with plaquette long-range order. Furthermore, we are able to link this phase to a consistent phase diagram of an extension of the SSM. Therefore, we introduce the quadrumerized SSM, defined on the square lattice by the following spin-1/2 Heisenberg Hamiltonian:

$$H = K \sum_{\langle i,j\rangle_\square} \mathbf{S}_i \cdot \mathbf{S}_j + J \sum_{\langle i,j\rangle_{\square'}} \mathbf{S}_i \cdot \mathbf{S}_j + J' \sum_{\langle\langle i,j\rangle\rangle} \mathbf{S}_i \cdot \mathbf{S}_j . \quad (1)$$

Here K and J are the two inequivalent nearest-neighbor exchange couplings, whereas J' denotes the next-nearest-neighbor alternating dimer coupling. The various couplings are displayed in Fig. 1.

Note that the lattice is self-dual under the exchange $(J \leftrightarrow K)$, hence only the case $J \leqslant K$ will be considered. Furthermore, the standard Shastry-Sutherland model is recovered along $J=K$, and has a larger space-group symmetry. Other lines of enhanced symmetry correspond to the 1/5th depleted square lattice $(J=0)$, and the plaquette square lattice $(J'=0)$, respectively.

The paper is organized as follows: In the next section we present the phase diagram of the quadrumerized SSM as obtained from boson operator mean-field theory. Then in the third section we use exact numerical diagonalization to study the effects of frustration in the model and relate the numerical results to the mean-field phase diagram. We concentrate on the standard SSM in the fourth section and provide evidence for a VBC intermediate phase. A summary and conclusions are given in the final section.

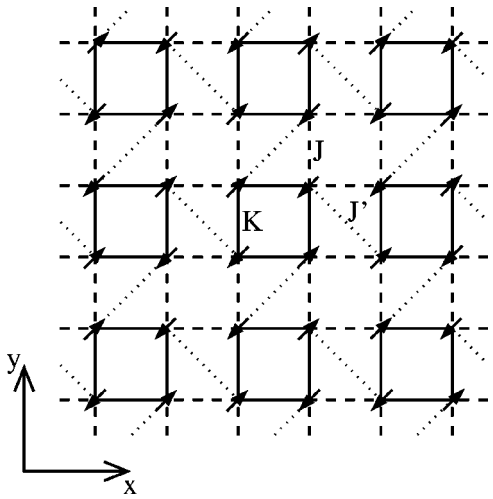

FIG. 1. The quadrumerized Shastry-Sutherland lattice. A spin-1/2 degree of freedom is located on each vertex. The various couplings, represented by different line styles, are denoted by K (solid), J (dashed), and J' (dotted). The lattice is self-dual under the exchange $(J \leftrightarrow K)$. Arrows illustrate the ordered phase found for $J=0$ in the region $J' \approx K$.

II. BOSON OPERATOR APPROACH

We first review the numerical results obtained along the unfrustrated lines in the parameter space of the Hamiltonian (1). For the 1/5th depleted square lattice ($J=0$) there exists a plaquette RVB-like phase (PRVB) at small $J'/K<0.94$, and a dimer RVB-like phase (DRVB) at large $J'/K>1.67$, with an intermediate long-range-order antiferromagnetic phase.[4] The classical configuration corresponding to this order is depicted by the arrows in Fig. 1.

The plaquette square lattice ($J'=0$) is unfrustrated as well. Using stochastic series-expansion quantum Monte Carlo simulations a quantum critical point is found at $(J/K)_c \approx 0.55$, separating a PRVB spin liquid for $J/K<(J/K)_c$ from a gapless Néel-ordered phase.[13] This value agrees well with results from perturbation expansions.[14]

While quantum Monte Carlo proves powerful for studying the unfrustrated limits of the Hamiltonian (1), due to the sign problem other methods are needed, once frustration is present. In order to study possible instabilities of the spin liquid phases, we use standard boson operator mean-field theory, which is known to work on a qualitative level even for large frustration. Our analytical results will also be substantiated by the numerical approach of the following sections.

A. Dimer-boson approach

Consider first the DRVB regime $J' \gg J,K$ where the dimer-boson technique can be applied.[15] In this representation, the spin-1/2 degrees of freedom on each J' dimer are expressed by bosonic bond operators,

$$|s\rangle = s^\dagger|0\rangle = |0,0\rangle,$$

$$|t_+\rangle = t_+^\dagger|0\rangle = |1,-1\rangle,$$

$$|t_0\rangle = t_0^\dagger|0\rangle = |1,0\rangle,$$

$$|t_-\rangle = t_-^\dagger|0\rangle = |1,+1\rangle, \tag{2}$$

where the $|S,S^z\rangle$ denote the states on a given dimer. From the action of the spin operators $\mathbf{S}_i$, $i=1,2$ (denoting the two sites of a dimer) on these states the representation of the spin operators can be deduced as

$$S_i^z = \frac{1}{2}(t_+^\dagger t_+ - t_-^\dagger t_-) - \frac{(-1)^i}{2}(t_0^\dagger s + s^\dagger t_0),$$

$$S_i^\pm = \frac{1}{\sqrt{2}}(t_\pm^\dagger t_0 + t_0^\dagger t_\mp) \pm \frac{(-1)^i}{\sqrt{2}}(t_\pm^\dagger s - s^\dagger t_\mp). \tag{3}$$

The spin commutation relations for $\mathbf{S}_i$, $i=1,2$ are obtained when the bond operators obey bosonic statistics. Furthermore, the number of physical states available on each dimer specifies a hard-core constraint for the bosons on each dimer μ,

$$s_\mu^\dagger s_\mu + t_{\mu,+}^\dagger t_{\mu,+} + t_{\mu,0}^\dagger t_{\mu,0} + t_{\mu,-}^\dagger t_{\mu,-} = 1. \tag{4}$$

Taking the interdimer couplings J and K into account and using Eq. (3), the Hamiltonian (1) is mapped onto an equivalent bosonic Hamiltonian, $H^D = H_0^D + H_I^D$, containing quadratic, diagonal terms

$$H_0^D = J' \sum_\mu -\frac{3}{4} s_\mu^\dagger s_\mu + \frac{1}{4}(t_{\mu,+}^\dagger t_{\mu,+} + t_{\mu,0}^\dagger t_{\mu,0} + t_{\mu,-}^\dagger t_{\mu,-}),$$

and quartic terms H_I^D describing the interdimer scattering. The square lattice of dimers, with two dimers per unit cell, is found to reduce to a square lattice with a single site per unit cell in the bosonic representation. Here, we first imagine rotating half of the J' dimers clockwise, so that all dimers align along the $(1,-1)$ direction (cf. Fig. 1). Then we take the centers of the dimers as the sites and use a coordinate system where x_D is along the original $(1,-1)$ direction and y_D along (1,1). To proceed, we need to implement the constraint (4) by means of a Holstein-Primakoff representation,[16]

$$s^\dagger = s = \sqrt{1 - t_+^\dagger t_+ - t_0^\dagger t_0 - t_-^\dagger t_-},$$

and then decouple the quartic H_I^D via a linear approximation, similar to linear spin-wave theory. The resulting total quadratic Hamiltonian, $\bar{H}^D$, is then diagonalized in momentum space using a generalized Bogoliubov transformation.[17] This approach is expected to work well inside the DRVB phase. A threefold-degenerate spectrum of triplet excitations is obtained, consistent with unbroken SU(2) symmetry,

$$\omega(\mathbf{k}_D) = \sqrt{J'[J' + (K-J)(\cos k_x - \cos k_y)]}. \tag{5}$$

Here, the wave vector $\mathbf{k}_D = (k_x, k_y)_D$ is defined with respect to the dimer coordinate system (x_D, y_D). The phase boundaries of the DRVB phase are obtained from the instabilities of the triplet excitation spectrum, i.e., by a vanishing spin gap at $\mathbf{k}_D = (\pi,0)_D$, signaling the condensation of the corresponding bosons at this wave vector.[15] Mapping back onto the original square lattice, the corresponding magnetic order is obtained, characterizing the phase beyond the instability line $2(K-J) \geqslant J'$. In fact, this magnetic order corresponds to the long-range order found for the 1/5th depleted square lattice, cf. Fig. 1.

B. Quadrumer-boson approach

When the parameters in the Hamiltonian of Eq. (1) are close to another limiting case, $J,J' \ll K$, a similar approach, the quadrumer-boson technique, can be applied.[18] The Hamiltonian of a single quadrumer, $H = K[\mathbf{S}_1 \cdot \mathbf{S}_2 + \mathbf{S}_2 \cdot \mathbf{S}_3 + \mathbf{S}_3 \cdot \mathbf{S}_4 + \mathbf{S}_4 \cdot \mathbf{S}_1]$, can be expressed in terms of the total spin, $\mathbf{S} = \mathbf{S}_1 + \mathbf{S}_2 + \mathbf{S}_3 + \mathbf{S}_4$, and the total subspin on each diagonal, $\mathbf{S}_A = \mathbf{S}_1 + \mathbf{S}_3$, and $\mathbf{S}_B = \mathbf{S}_2 + \mathbf{S}_4$. The spectrum is given by $E(|S,S^z,S_A,S_B\rangle) = K/2(S^2 - S_A^2 - S_B^2)$. The lowest-lying triplet $\{|1,S^z,1,1\rangle, S^z = 0,\pm 1\}$ has a gap, $\Delta = K$, to the ground state $|0,0,1,1\rangle$. Since there is a further gap, $\Delta' = K$, to the higher excitations, we attempt to obtain the instabilities of the PRVB phase by using a restricted quadrumer-boson method, omitting all the higher excitations on the quadrum-

ers. Hence, the spin-1/2 degrees of freedom on each quadrumer are expressed by bosonic operators on the restricted Hilbert space,

$$|s\rangle = s^\dagger|0\rangle = |0,0,1,1\rangle,$$

$$|t_+\rangle = t_+^\dagger|0\rangle = |1,-1,1,1\rangle,$$

$$|t_0\rangle = t_0^\dagger|0\rangle = |1,0,1,1\rangle,$$

$$|t_-\rangle = t_-^\dagger|0\rangle = |1,+1,1,1\rangle. \quad (6)$$

From the action of the spin operators $\mathbf{S}_i$, $i=1,\ldots,4$ in the restricted Hilbert space, the following representation can be deduced:[19]

$$S_i^z = \frac{1}{4}(t_+^\dagger t_+ - t_-^\dagger t_-) - \frac{(-1)^i}{\sqrt{6}}(t_0^\dagger s + s^\dagger t_0),$$

$$S_i^\pm = \frac{1}{2\sqrt{2}}(t_\pm^\dagger t_0 + t_0^\dagger t_\mp) \pm \frac{(-1)^i}{\sqrt{3}}(t_\pm^\dagger s - s^\dagger t_\mp). \quad (7)$$

In the restricted Hilbert space, the hard-core constraint (4) is now obeyed on each quadrumer. Expressing the Hamiltonian (1) in terms of the quadrumer-boson operators, a bosonic Hamiltonian, $H^P = H_0^P + H_I^P$, is obtained with a noninteracting diagonal part

$$H_0^P = K\sum_\mu -2s_\mu^\dagger s_\mu - (t_{\mu,+}^\dagger t_{\mu,+} + t_{\mu,0}^\dagger t_{\mu,0} + t_{\mu,-}^\dagger t_{\mu,-})$$

and a quartic scattering part H_I^P. Here the sum extends over the square lattice of quadrumers formed by the K bonds in Fig. 1. Following the decoupling procedure already used in the dimer-boson approach, the following threefold-degenerate triplet excitation spectrum is obtained in the PRVB regime,

$$\omega(\mathbf{k}_P) = \sqrt{K\left[K - \frac{2}{3}(2J - J')(\cos k_x + \cos k_y)\right]}. \quad (8)$$

The minimum of this spectrum is located at $\mathbf{k}_P = (\pi,\pi)_P$ when $J' > 2J$, and the gap vanishes for $J' > 3/4(K+2J)$, corresponding again to the order depicted in Fig. 1. Furthermore, for $J' < 2J$ the minimum is located at $\mathbf{k}_P' = (0,0)_P$, and the gap is again closed for $J' < 2J - 3/4K$. In this regime the model becomes long-range Néel ordered.

Upon comparing the ground-state energies from the dimer- and the quadrumer-boson approaches inside the common range of stability, we can obtain the direct first-order transition line between the DRVB and PRVB spin liquid phases.[18]

The overall phase diagram is shown in Fig. 2. The spin liquid phases are characterized by the corresponding RVB-like state, while we label the long-range ordered phases by the ordering wave vectors in the boson operator approaches. Furthermore, solid lines represent second-order phase transitions, whereas the dashed line indicates the first-order transition line.

The Néel-ordered phase $(0,0)_P$ extends up to rather large frustration, with the largest extent of $(J'/J)_{\max} \approx 1.2$ along the Shastry-Sutherland line ($J=K$). On the other hand, the largest extent of the $(\pi,\pi)_P$ phase, for $J'/K \approx 1.3$, is bound by $(J/K)_{\max} < 0.55$ from exact diagonalization. This difference can be traced back to the ratio of the number of frustrating couplings to the number the initial couplings, which is 1:4 when starting at $J'=0$, but 2:3 upon starting at $J=0$.

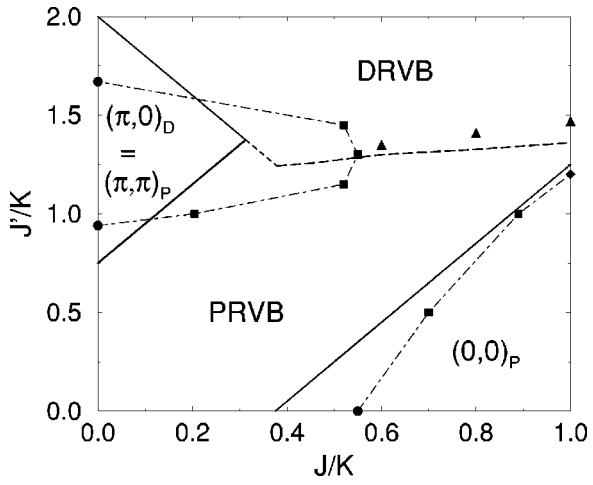

FIG. 2. Phase diagram of the quadrumerized Shastry-Sutherland model. Ordered phases are characterized by the ordering wave vectors in the boson representations. Solid lines indicate second-order transition lines, and the dashed line the first-order transition. Also shown are points on the phase boundaries from quantum Monte Carlo (circles), (Refs. 4 and 13) exact diagonalization (squares and triangles), and series expansion (diamonds) (Ref. 12). Dash-dotted lines are guides to the eye. The increment of the parameter scan in exact diagonalization was $\Delta(J/K)=0.1$ [$\Delta(J'/K)=0.2$] for the $(\pi,\pi)_P$ [$(0,0)_P$] phase boundary.

Furthermore, from the phase diagram in Fig. 2, we find that the DRVB phase of the 1/5th depleted square lattice is adiabatically connected to the exact dimer VBS phase of the standard Shastry-Sutherland model (the dimer VBS state fails to be an exact eigenstate for $J \neq K$). On the other hand, the DRVB phase is not adiabatically connected to the PRVB, as expected on topological grounds.[21] Hence, we find a first-order phase transition separating the two spin liquid phases beyond the regime of the $(\pi,\pi)_P$ phase.

When turning to the case $J>K$, the phase diagram shown in Fig. 2 is obtained upon interchanging J and K, due to the invariance of the Hamiltonian in Eq. (1) under the exchange ($J \leftrightarrow K$). Furthermore, we label the plaquette RVB-like phase for $J>K$ by PRVB′, since now singlets are predominantly formed on a different set of quadrumers than in the PRVB phase.

III. EXACT DIAGONALIZATION STUDIES

We include in Fig. 2 the positions of quantum critical points along the unfrustrated lines, obtained by quantum Monte Carlo simulations.[4,13] These compare rather well with the above mean-field theory. To extend the numerical analysis into the frustrated regime we have performed exact diagonalization studies on clusters with $N=8, 16$, and 32 spins, using periodic boundary conditions, along various

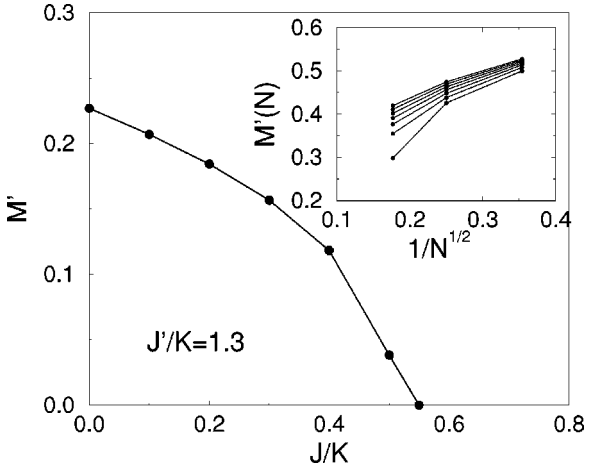

FIG. 3. Evolution of the order parameter of the $(\pi,\pi)_P$ phase upon increasing J/K for $J'/K=1.3$. The inset shows the finite-size data obtained for $N=8$, 16, and 32 at $J/K=0$, 0.1, . . . , 0.6 (top to bottom).

lines in the phase diagram. We determine the finite-size values of the order parameter, M', defined by[20]

$$M'^2(N)=\frac{1}{N(N+2)}\left\langle\left(\sum_i \epsilon_i \mathbf{S}_i\right)^2\right\rangle. \tag{9}$$

Here ϵ_i takes on the values ± 1 at site i, according to the pattern in Fig. 1 for the $(\pi,\pi)_P$ phase or the standard Néel order for the $(0,0)_P$ phase, respectively. Using the finite-size data we determine M' from the scaling law[20]

$$M'(N)=M'+\frac{c_1}{N^{1/2}}+\frac{c_2}{N}. \tag{10}$$

For example, in Fig. 3 we show results obtained along the line $J'=1.3$, where quantum Monte Carlo simulations at $J=0$ give a maximum moment of $M'\approx 0.23$.[4] Within exact diagonalization we can reproduce this value, and furthermore observe a smooth decrease in M' upon increasing the frustration, up to a critical point at $J/K\approx 0.55$, where we enter into the spin liquid regime. Proceeding in a similar fashion we obtain the critical points depicted by squares in Fig. 2. Moreover, along the line $J'=2J$ no finite order parameter was obtained after finite-size scaling.

The two spin liquid phases cannot be separated within exact diagonalization using space-group symmetry. Namely, upon increasing J'/K for a constant J/K, the representation class of the ground state does not change. Nevertheless, from the approximate slopes of the ground-state energy vs J'/K at constant J/K in the regions of small and large J'/K, respectively, we estimated the first-order transition points indicated by triangles in Fig. 2.

Comparing these numerical results with the mean-field calculations in the last section, we conclude that the boson operator approach gives a good qualitative account of the phase diagram of the quadrumerized SSM. Namely, the characterization of the various phases and the location of the phase-transition lines agree well with numerical results.

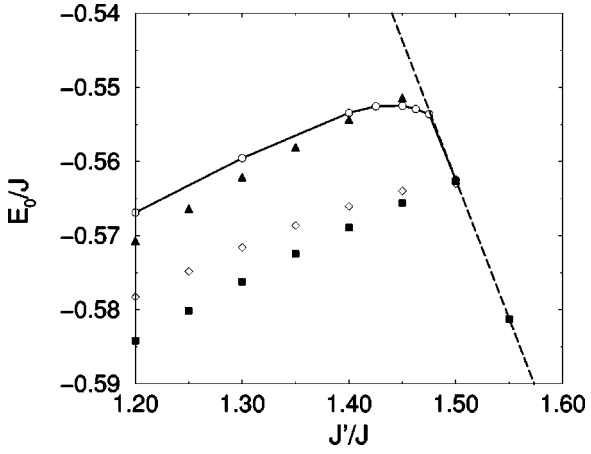

FIG. 4. Ground-state energy per site of the Shastry-Sutherland model from exact diagonalization of clusters with $N=16$ (squares), 20 (triangles), 24 (diamonds), and 32 (circles) sites. The solid line is a guide to the eye, and the dashed line is the exact dimer VBS state energy.

IV. SHASTRY-SUTHERLAND MODEL

In the quadrumer-boson approach we find a finite window on the Shastry-Sutherland line $(J=K)$, where both plaquette spin liquid phases, PRVB and PRVB′, come arbitrary close to the $J=K$ line. This already indicates an intermediate phase in the standard SSM between the Néel-ordered phase and the dimer VBS phase. Similar conclusions were obtained in a field-theoretical study of a generalized SSM, which does not break the symmetry needed by the dimer VBS state to be an exact eigenstate.[11] We now focus on this intermediate regime in the standard SSM.

There has recently been considerable interest in the nature of the intermediate phase. In the large spin, classical limit the system retains Néel order for $J'/J\leqslant 1$ and is helically ordered otherwise, with a twist between next-nearest-neighbor spins of $q=\arccos(-J/J')$. Using Schwinger boson mean-field theory, Albrecht and Mila predicted the existence of a helical phase separating the dimer VBS and the ordered phase also for the spin-1/2 case, in a range $1.1<J'/J<1.65$.[8] Field-theoretical studies by Chung, Marston, and Sachdev for a generalized spin-S model with $Sp(2N)$ symmetry suggest the helical order to occur in a larger range, $1.02<J'/J<2.7$, at $S=1/2$.[10] Furthermore, this approach predicts a phase with plaquette order in the extreme quantum limit, $1/S>5$. Indeed, using series expansions around the plaquette limit of Eq. (1), Koga and Kawakami found the intermediate phase in a range $1.16<J'/J<1.48$ to be adiabatically connected to the PRVB phase.[9] However, extended series expansions by Zheng, Oitmaa, and Hamer lead to different conclusions.[12] They suggest the PRVB phase to become unstable before the Shastry-Sutherland line is reached and found a columnar dimer phase to be a possible candidate for the intermediate phase.

Here, we perform exact diagonalization studies on clusters with up to 32 sites, significantly beyond the largest cluster sizes studied so far (24 sites in Ref. 22). In Fig. 4 we show the ground-state energy of the SSM close to the tran-

sition into the dimer VBS state for various cluster sizes. The solid line shows our results for the 32 site cluster, whereas other sizes are represented by symbols. In addition, the energy of the dimer VBS state is shown by the dashed line. Due to the different symmetry of the various clusters, the ground-state energy per site does not show a monotonous finite-size dependence. Nevertheless, independent of the cluster size we find the system to be within the dimer VBS for $J'/J>1.5$, consistent with the upper bound for the intermediate phase given by Koga and Kawakami, but significantly below the values from the Schwinger boson, and $Sp(2N)$ theory. From finite-size analysis of the Néel-order parameter, we estimate a upper bound for the ordered phase of $(J'/J)_{\max}<1.4$, consistent with the series-expansion value $(J'/J)_{\max}=1.2\pm0.1$.[12] More interestingly, for the largest cluster we find a characteristic change in the curvature of the ground-state energy, well before entering the dimer VBS. Hence, we conclude that characteristic features of the intermediate phase could be retrieved from clusters with $N=32$ sites in a range $1.425<J'/J<1.475$. In this regime we find the spin-spin, or two-point correlation function to decrease rapidly with distance, indicating the absence of antiferromagnetic order.

In order to test against the various proposed ground states, we measure the dimer-dimer or four-point correlation functions,

$$C^4(i,j,;k,l)=\langle \mathbf{S}_i\cdot\mathbf{S}_j\mathbf{S}_k\cdot\mathbf{S}_l\rangle-\langle \mathbf{S}_i\cdot\mathbf{S}_j\rangle\langle \mathbf{S}_k\cdot\mathbf{S}_l\rangle, \qquad (11)$$

on the $N=32$ lattice in the above interaction range. In particular, we fix $(i,j)=(0,16)$ and extend (k,l) over all inequivalent J bonds. The values obtained in the ground state for $J'/J=1.45$ are displayed in Table I, and illustrated in Fig. 5, which also shows the labeling of the sites.

We obtain a clear signal in the dimer-dimer correlations that extends throughout the whole cluster, with a finite asymptotic value approximately reached for the larger dimer-dimer distances on the cluster. In the spatial distribution we furthermore observe periodic oscillations, which reflect an underlying order of quadrumer singlets, formed predominately on void squares (i.e., those squares not containing a diagonal bond).

For the SSM there are two equivalent configurations with quadrumer-singlet coverings residing on the two different subsets of void squares (formed by the J or K bonds in Fig. 1, respectively). Hence, if the plaquettelike order in the four-spin correlation function survives quantum fluctuations, indicative of a plaquette VBC, a twofold-degenerate ground-state manifold will emerge in the thermodynamic limit. On a finite lattice this degeneracy is lifted, but a low-lying singlet state well inside the triplet gap and only slightly above the ground-state energy is expected. We can obtain the quantum numbers of this singlet state from the following symmetry considerations: The Shastry-Sutherland lattice has a $p4mm$ space-group symmetry,[23] and the ground state of the 32 site cluster has momentum $\mathbf{k}=(0,0)$, and is invariant under the $\pi/2$ rotations about the center of any void square (i.e., s wavelike). Furthermore, the two equivalent configurations of quadrumer-singlet coverings are related by the reflections about either diagonal dimer axis, but are invariant under the $\pi/2$ rotations and lattice translations. Namely, they both reside already inside a single unit cell of the Shastry-Sutherland lattice.

TABLE I. Dimer-dimer correlations $C^4(1,2;k,l)$ in the ground state of the Shastry-Sutherland model on the 32 site cluster at $J'/J=1.45$. The labeling of the sites is shown in Fig. 5.

(k,l)	$C^4(0,16;k,l)$	(k,l)	$C^4(0,16;k,l)$
25 , 26	0.0213	20 , 26	0.0140
29 , 30	0.0222	21 , 27	0.0180
31 , 9	0.0788	22 , 1	0.0274
2 , 3	0.0825	17 , 23	0.0152
6 , 7	0.0222	18 , 24	0.0148
12 , 13	0.0209	8 , 14	0.0175
8 , 28	0.0140	28 , 15	0.0239
14 , 15	0.0144	29 , 31	0.0274
21 , 22	0.0140	9 , 30	0.0152
1 , 27	0.0153	4 , 10	0.0239
4 , 5	0.0138	5 , 11	0.0175
10 , 11	0.0160	6 , 12	0.0148
17 , 18	0.0140	7 , 13	0.0180
23 , 24	0.0214	19 , 25	0.0140
19 , 20	0.0223	13 , 20	−0.0124
24 , 25	−0.0107	14 , 21	−0.0143
28 , 29	−0.0104	15 , 22	−0.0207
15 , 31	−0.0007	10 , 17	−0.0019
1 , 2	−0.0007	11 , 18	−0.0135
5 , 6	−0.0137	27 , 4	−0.0177
11 , 12	−0.0107	1 , 5	−0.0177
30 , 4	−0.0104	2 , 6	−0.0019
9 , 10	−0.0292	3 , 7	−0.0207
3 , 23	−0.0292	23 , 8	−0.0103
7 , 8	−0.0137	24 , 28	−0.0164
13 , 14	−0.0163	25 , 29	−0.0142
20 , 21	−0.0125	26 , 30	−0.0135
26 , 27	−0.0163	12 , 19	−0.0138
18 , 19	−0.0125		

Hence, a low-lying s-wave symmetric singlet state with momentum (0,0) is expected to be included in the spectrum of the 32 site cluster in the regime of the plaquette VBS phase. This state should furthermore show similar dimer-dimer correlations as the absolute ground state.

In Fig. 6 we plot the ground-state energy along with those of the lowest excited singlet and triplet states for the 32 site cluster in the zero-momentum sector. We specify the transformation properties of the various states under the $\pi/2$ rotation by the eigenvalue $R_{\pi/2}=1$ (s wave), -1 (d wave), or $\pm i$ (twofold degenerate). See the caption of Fig. 6 for a detailed account on the various symbols used. In the regime where we expect evidence for an intermediate state we indeed find various low-lying singlet states well inside the rather large triplet gap. Moreover, there are two singlet states with energies rather close to the ground-state energy, one being an s-wave, and the other a d-wave state with respect to the $\pi/2$ rotations. We furthermore calculated the dimer-dimer

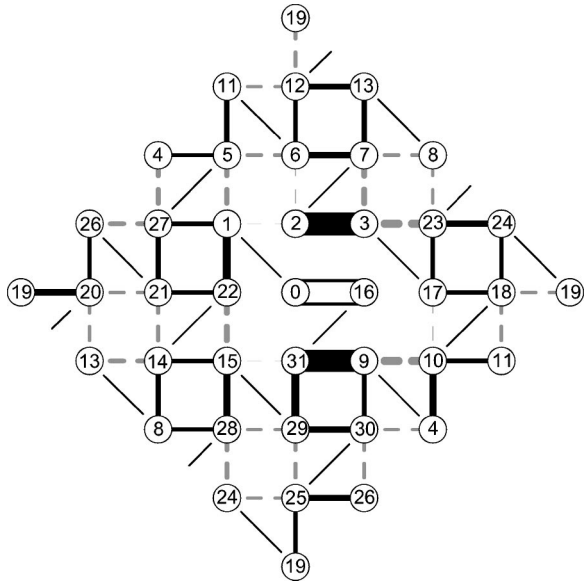

FIG. 5. Dimer-dimer correlations in the ground state of the Shastry-Sutherland model on the 32 site cluster at $J'/J=1.45$. The reference bond is the bond (0,16). Positive (negative) correlations are drawn as full (dashed) lines. The thickness of a line is proportional to the strength of the correlation. Short diagonal lines indicate the position of the J'-dimer bonds.

correlations for both states and find for the *s*-wave state a similar signal as for the absolute ground state. On the other hand, the *d*-wave state does not show any pattern in the dimer-dimer correlations. This state does not seem relevant for the ground state of the system in the thermodynamic limit. Presumably it is related to low-lying excitations in the dimer VBS phase.[22,23]

From the above we conclude that the low-lying *s*-wave singlet state, having the right quantum numbers and dimer-dimer correlation, will become degenerate with the ground state upon increasing the cluster size to the infinite lattice. Both states then form the twofold-degenerate ground-state manifold of a plaquette VBC in the thermodynamic limit. In Fig. 7 a pictorial description of this ground-state manifold is given. Furthermore, this ground-state manifold is invariant with respect to lattice translations and the $\pi/2$ rotations about the centers of the void squares, but each state spontaneously breaks the reflection symmetry about the diagonal axes along the dimer directions. From our numerical results we can also exclude a columnar dimer state, which would be fourfold degenerate and furthermore show a different pattern in the dimer-dimer correlations than depicted in Fig. 5.[26]

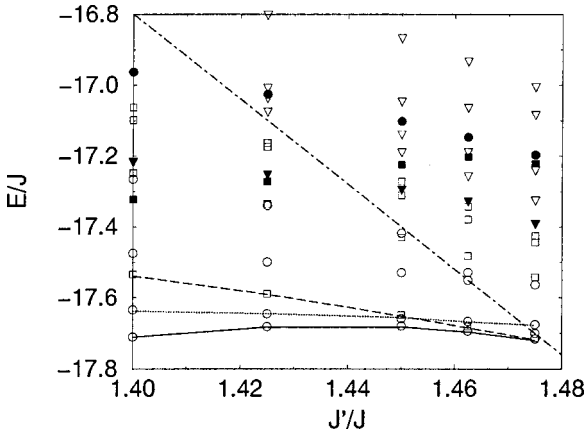

FIG. 6. Ground-state energy, and low-lying singlet and triplet excitations in the $\mathbf{k}=(0,0)$ sector of the Shastry-Sutherland model on the 32 site cluster. Open symbols represent singlet states, full symbols triplet states. Circles denote states with eigenvalues $R_{\pi/2}=1$ (*s* wave), squares denote $R_{\pi/2}=-1$ (*d* wave), and triangles $R_{\pi/2}=\pm i$ (two fold degenerate). The solid line is a guide to the eye for the ground state, the dotted line to the lowest excited *s*-wave state, and the dashed line the lowest *d*-wave state. The dash-dotted line is the exact dimer VBS state energy.

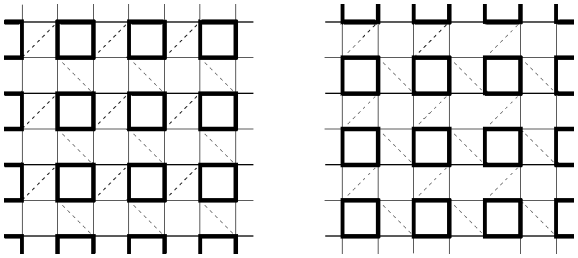

FIG. 7. Pictorial illustration of the variational ground-state manifold of the Shastry-Sutherland model in the plaquette VBC phase. Thick lines indicate four spins involved in a quadrumer singlet.

Further evidence for the relevance of the plaquette VBC in the intermediate regime of the SSM can be drawn from analogous results of recent studies on the spin-1/2 Heisenberg model on the checkerboard lattice.[24,25] In this model, diagonal bonds are again organized on a square lattice in a pattern that leaves half of the squares void. Namely, the underlying lattice is obtained by adding in an additional diagonal bond on each square on which a dimer bond is located in Fig. 1. Also in the checkerboard lattice quadrumer singlets form on the void squares, resulting in a two fold-degenerate plaquette VBC ground-state manifold with broken space-group symmetry. The structure leading to frustration is rather similar in both models, and the system tries to minimize frustration by forming plaquette valence bonds on the void squares. Due to the homogeneous axial couplings, this can be accomplished only upon spontaneously breaking the symmetry inherited from the underlying lattice.

V. CONCLUSIONS

In conclusion, we have studied the phase diagram of the quadrumerized Shastry-Sutherland model. Using bond-operator methods and exact numerical diagonalization its phase diagram was established, which links the various results available for special limiting cases of the model. The antiferromagnetically ordered phase of the 1/5th depleted square lattice model is destroyed by modest frustration, whereas the Néel-ordered phase extends up to rather large frustration. There is a first-order transition line separating the different spin liquid phases, PRVB and DRVB, beyond the ordered phase. Furthermore, the DRVB is adiabatically connected to the dimer VBS phase of the SSM.

For the standard SSM there exists a finite region around

$J'/J=1.45$ where the system becomes a plaquette VBC with spontaneously broken space-group symmetry, and a twofold-degenerate ground-state manifold. Perturbing away from the Shastry-Sutherland line, i.e., for $J \neq K$, the symmetry is broken explicitly, and the system favors a unique ground state, namely, the PRVB for $J<K$, and the PRVB$'$ for $J>K$. Furthermore, upon varying J' along the Shastry-Sutherland line, a first-order transition leads to the dimer VBS and a second-order transition to the Néel-ordered phase. Within our analytical and numerical studies we did not find indications for further phases in the (quadrumerized) SSM.

Stabilization of a plaquette VBC phase in both the Shastry-Sutherland and the checkerboard lattice model agrees with the generic structure of the underlying frustrated lattice. However, in the SSM the VBC is unstable towards the dimer VBS upon increasing the diagonal coupling. For the checkerboard lattice model the range of the VBC phase is still unknown, and remains for further studies.

Note added. After completion of this work Akihisa Koga and Norio Kawakami pointed us to Ref. 27, where the phase diagram of the Hamiltonian in Eq. (1) was studied using series-expansion methods. Their results are in perfect agreement with our calculations in Secs. II and III. However in Ref. 27 the VBC nature of the intermediate phase in the Shastry-Sutherland model was not noticed.

ACKNOWLEDGMENTS

We acknowledge fruitful discussions with Stephan Haas, Andreas Honecker, and Bruce Normand. This work has been financially supported by the Swiss National Fonds.

[1] For a recent review, see, e.g., C. Lhuillier and G. Misguich, cond-mat/0109146 (unpublished).
[2] K. Ueda, H. Kontani, M. Sigrist, and P.A. Lee, Phys. Rev. Lett. **76**, 1932 (1996).
[3] N. Katoh and M. Imada, J. Phys. Soc. Jpn. **64**, 4105 (1995).
[4] M. Troyer, H. Kontani, and K. Ueda, Phys. Rev. Lett. **76**, 3822 (1996); M. Troyer, M. Imada, and K. Ueda, J. Phys. Soc. Jpn. **66**, 2957 (1997).
[5] H. Kageyama, K. Yoshimura, R. Stern, N.V. Mushnikov, K. Onizuka, M. Kato, K. Kosuge, C.P. Slichter, T. Goto, and Y. Ueda, Phys. Rev. Lett. **82**, 3166 (1999).
[6] S. Miyahara and K. Ueda, Phys. Rev. Lett. **82**, 3701 (1999).
[7] B.S. Shastry and B. Sutherland, Physica B & C **108B**, 1069 (1981).
[8] M. Albrecht and F. Mila, Europhys. Lett. **34**, 145 (1996).
[9] A. Koga and N. Kawakami, Phys. Rev. Lett. **84**, 4461 (2000).
[10] C.H. Chung, J.B. Marston, and S. Sachdev, Phys. Rev. B **64**, 134407 (2001).
[11] D. Carpentier and L. Balents, Phys. Rev. B **65**, 024427 (2002).
[12] Weihong Zheng, J. Oitmaa, and C.J. Hamer, Phys. Rev. B **65**, 014408 (2002).
[13] S. Wessel (unpublished).
[14] Y. Zukumoto and A. Oguchi, J. Phys. Soc. Jpn. **67**, 2205 (1998).
[15] S. Sachdev and R.N. Bhatt, Phys. Rev. B **41**, 9323 (1990).
[16] A.V. Chubukov and Th. Jolicoeur, Phys. Rev. B **44**, 12 050 (1991).
[17] Th. Jolicoeur and J.C. Guillou, Phys. Rev. B **40**, 2727 (1989).
[18] O.A. Starykh, M.E. Zhitomirsky, D.I. Khomskii, R.R.P. Singh, and K. Ueda, Phys. Rev. Lett. **77**, 2558 (1996).
[19] Keeping all excited states and the corresponding bosons, 26 more bilinear terms appear for each spin operator.
[20] M. Albrecht, F. Mila, and D. Poilblanc, Phys. Rev. B **54**, 15 856 (1996).
[21] N.E. Bonesteel, Phys. Rev. B **40**, 8954 (1989).
[22] K. Totsuka, S. Miyahara, and K. Ueda, Phys. Rev. Lett. **86**, 520 (2001).
[23] C. Knetter, A. Bühler, E. Müller-Hartmann, and G.S. Uhrig, Phys. Rev. Lett. **85**, 3958 (2000).
[24] J.-B. Fouet, M. Mambrini, P. Sindzingre, and C. Lhuillier, cond-mat/0108070 (unpublished).
[25] W. Brenig and A. Honecker, Phys. Rev. B **65**, 140407(R) (2002).
[26] P.W. Leung and N. Lam, Phys. Rev. B **53**, 2213 (1996).
[27] Y. Takushime, A. Koga, and N. Kawakami, J. Phys. Soc. Jpn. **70**, 1369 (2001).